

Direct Oxidation of Methane to Methanol Enabled by Electronic Atomic Monolayer–Metal Support Interaction

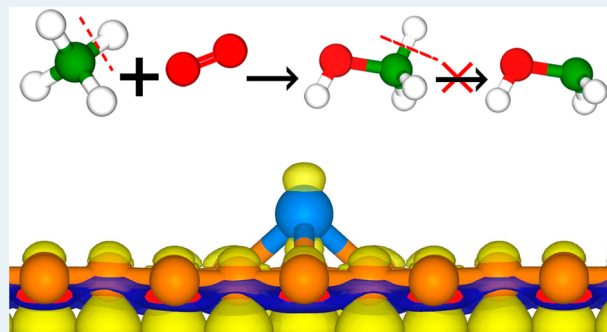
Yongjie Xi and Andreas Heyden*

Department of Chemical Engineering, University of South Carolina, 301 South Main Street, Columbia, South Carolina 29208, United States

Supporting Information

ABSTRACT: Direct, catalytic oxidation of methane to methanol (MTM) with molecular oxygen is a highly desirable process to valorize methane. We propose that Rh-doped graphene (GR) supported on Ni(111) can be a promising catalyst for MTM with appreciable activity and selectivity. In the absence of the Ni(111) support, a MTM process is difficult. The catalytic activity of the Rh-doped GR is enabled by the Ni(111) support that covalently binds the Rh-doped GR and significantly modifies its properties, leading to facile O_2 activation by the synergy of the Rh dopant and the neighboring carbon atom of GR. The highly activated O_2 and the Rh dopant in turn activate CH_4 . Strikingly, the methane C–H bond breaking is preferred over methanol C–H bond breaking at 473 K. The strong interaction between TM-doped GR and Ni(111) is found to be a general mechanism for regulating the adsorption strength of various molecules, providing important insight for tuning the properties of single-atom catalysts.

KEYWORDS: methane to methanol conversion, single atom catalyst, graphene, support interaction, DFT calculation



INTRODUCTION

The increasing supply of natural gas and the resulting increased cost differential between natural gas and petrochemicals that can be derived from natural gas make the development of efficient heterogeneous catalysts for transforming methane into value-added fuels and chemicals an appealing value proposition. Direct oxidation of methane to methanol (MTM) with molecular oxygen is the economically preferred approach for valorizing methane relative to indirect oxidation processes involving the energy-intensive syngas production or the use of other (more expensive or corrosive) oxidants. Despite active research for many decades, no economically viable direct MTM process has been developed on an industrial scale.¹

A prerequisite for a potential MTM catalyst is the ability to efficiently activate both methane and dioxygen. Computational studies have correlated the C–H activation barriers of methane with the hydrogen adsorption energies over various heterogeneous catalysts.² The methane molecule is relatively inert and the C–H cleavage is difficult.³ The efficient activation of both CH_4 and O_2 at the same active site is even more challenging, explaining the lack of highly active MTM catalysts. While the reaction rate of the MTM catalyst can be increased with increasing reaction temperature, overoxidation occurs at high temperatures and it was suggested that optimal operating conditions are below 500 K.^{4,5} Copper-exchanged zeolites, mimicking the methane monooxygenase that catalyzes MTM in nature, are among the most extensively explored low temperature MTM catalysts in academia. Unfortunately, Cu-

exchanged zeolites suffers from low activity and the active sites usually need to be preoxidized at high temperatures before the methane oxidation can take place.^{4,6–8} Meaningful but still too low methane to methanol yields have recently been observed for mononuclear rhodium species anchored on a zeolite or TiO_2 support and suspended in aqueous solution.⁹

The need for developing more efficient MTM catalysts motivated us to search for new chemistries that might potentially overcome the deficiencies of existing catalysts. In general, the activity and selectivity of a catalyst can be modified by changing its composition or external environment. The effects of support,¹⁰ solvent,¹¹ applied electric field,¹² and strain¹³ can regulate the property of a catalyst significantly and have been harnessed to achieve desired catalytic activity. The well-known strong metal–support interaction (SMSI)¹⁴ is a typical support interaction, which usually implies the undesired encapsulation of an active metal by a few-layer metal oxide support (CeO_2 , TiO_2 , etc.) that blocks the activity of the metal. Closely related to SMSI is the recently proposed electronic metal–support interaction (EMSI),^{10,15} which implies that a metal catalyst experiences a favorable electronic perturbation by a metal oxide support that brings about higher activity. While the effect of a metal oxide involved in SMSI or EMSI has been extensively explored, the role of a metal as a

Received: April 19, 2019

Revised: May 30, 2019

Published: June 3, 2019

support is less commonly studied and inverse oxide/metal catalysts¹⁶ and the ability of a Mo(100) support to charge and activate Au atoms on few-layer MgO that was deposited on the Mo(100) surface¹⁷ are rare examples. Therefore, utilization of the effect of a metal support may open new opportunities for the design of MTM catalysts.

Graphene (GR)^{18,19} and other two-dimensional (2D) materials have seen broad catalytic applications.^{20,21} There are evidence showing that the basal plane of graphene can be catalytically active in the presence of a metal support due to electronic interactions between the graphene and the metal.^{22–24} A more general approach to utilize GR-like monolayers in catalysis is to immobilize transition metal (TM) atoms to form single-atom catalysts (SAC),^{25–27} which is a recently emerging frontier in heterogeneous catalysis that promises very high atom efficiency and the design of highly selective heterogeneous catalysts due to the uniformity of the active sites.^{28,29} While catalytic applications of TM-doped GR-like monolayer SACs have been extensive, the metal-supported counterpart has been rare.³⁰ Therefore, it is intriguing to examine the catalytic properties of a metal-supported graphene-like monolayer with an embedded TM atom for the MTM process. GR³¹ and its analogue hexagonal boron nitride (hBN)³² can be chemisorbed on Ni(111) due to the small lattice mismatches (GR, 2.46 Å; Ni(111), 2.49 Å; hBN, 2.51 Å). In our attempt to develop more efficient MTM catalysts and unleash the catalytic potential of GR/hBN and single TM atoms, we propose to immobilize TM atoms in graphene and hBN to form SACs, which are supported on Ni(111). Specifically, using first-principles calculations, we investigated the energy profiles of MTM reactions over Rh-⁹ and Cu-doped⁴ GR as well as Rh-doped hBN supported on Ni(111). As a boron vacancy is preferred over a nitrogen vacancy for hBN, we immobilize a Rh atom with B-defective hBN.³³ To generalize the effect of a metal support on the catalytic properties of atomic monolayer-anchored SACs, we also examined the adsorption energies of small molecules on free-standing atomic layer and Ni(111)-supported SACs.

RESULTS AND DISCUSSION

Adsorption of TM-Doped GR on Ni(111). The adsorption of a Rh-doped (4 × 4) GR (GR-Rh) supported on (4 × 4) Ni(111) is presented in Figure 1a. A Rh atom can be immobilized at the single vacancy of a GR with an adsorption energy (E_{ads}) of −1.90 eV. High activation barriers for metal atom diffusion of 2.2–2.5 eV have previously been reported for graphene immobilized metal atoms suggesting that these structures are highly stable.³⁴ A recent experimental study supports this high stability for a graphene-trapped Ni SAC for hydrogen and oxygen evolution.³⁵ The E_{ads} of GR-Rh on (4 × 4) Ni(111) was calculated to be −3.52 eV. The covalent interaction between GR-Rh and Ni(111) is reflected by significant charge accumulation between GR-Rh and Ni(111) and a downshift of the GR-Rh projected density of states (DOS) for GR-Rh/Ni(111) as compared with the free-standing one (Figure 1d). Similar DOS were also observed in a recent computational study of Co-doped graphene supported on Ni(111) for the oxygen reduction reaction (ORR).³⁰ Bader charge³⁶ calculations suggest that the GR-Rh layer composed of C₃₁Rh gains 1.58 le^{−1} from the Ni(111) support. The activation of O₂ over Rh(111)-supported graphene was reported previously.³⁷ In the present study, we examine the adsorption of one O₂ (Figure 1c) at the Rh site (O₂-a), GR-Rh

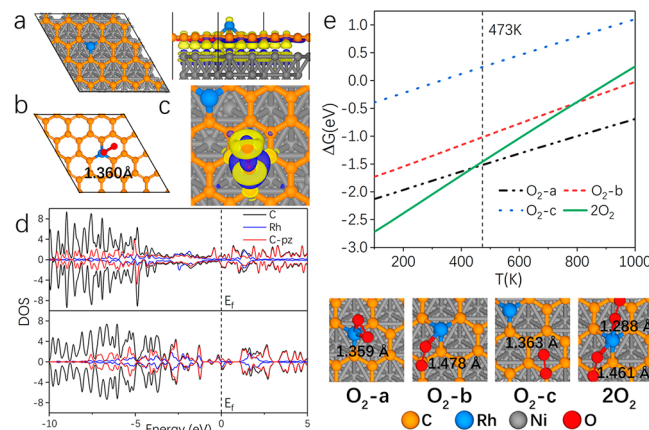


Figure 1. (a) Top and side view of a Rh-doped (4 × 4) GR supported on Ni(111). A carbon atom of pristine GR is substituted by a rhodium atom to create Rh-doped GR. The side view also displays the charge difference plot upon the adsorption of GR-Rh on Ni(111). The isosurface value is 0.003 le^{−1}/bohr³. The accumulation (depletion) of electrons is denoted by yellow (blue). (b) Adsorption of O₂ on free-standing GR-Rh. (c) Charge difference plot upon the adsorption of O₂ on a carbon site of GR-Rh/Ni(111). The isosurface value is 0.003 le^{−1}/bohr³. (d) Projected DOS of C and Rh for GR-Rh/Ni(111) and GR-Rh, respectively. Positive and negative values of DOS denote spin-up and spin-down electrons, respectively. (e) Results from constrained thermodynamic calculations of O₂ adsorption on GR-Rh/Ni(111). The O₂ partial pressure is 1 bar. O–O bond lengths are labeled.

interfacial site (O₂-b), and GR basal plane site (O₂-c), whose O₂ chemisorption energies are −2.34, −1.99, and −0.60 eV, respectively. At the interfacial site, the O–O bond length is elongated to 1.478 Å, as compared with the gas phase bond length of 1.234 Å. GR-Rh/Ni(111) can also accommodate another O₂ molecule in close vicinity of Rh(2O₂) with a total adsorption energy of −3.15 eV. In contrast, O₂ can only be adsorbed on the Rh site of free-standing GR-Rh with an adsorption energy of −2.03 eV while no C–O bond can be formed (Figure 1b). Bader charge calculations suggest that the O₂ of the configuration O₂-c gains 0.72 le^{−1} upon adsorption while charge redistributes at the C bonded to the O atoms as well as the three nearest-neighboring C atoms. The energetically favorable charge redistribution originates from the delocalized C p_z orbitals of GR-Rh/Ni(111) near the Fermi level, which are absent for GR-Rh such that the electron donation from the nonbonded C to O₂ is hindered.

Constrained thermodynamics calculations were performed to examine the stability of adsorbed oxygen at various temperatures and pressures. At an oxygen partial pressure of 1 bar and a typical operating temperature of 473 K, we found that O₂-a is the most stable adsorption configuration, which is 0.06 eV more stable than 2O₂. O₂-c is not stable at MTM operating conditions. While a chemisorbed O₂ that is activated to a greater extent might be more active for CH₄ activation, we considered the O₂-a, O₂-b, and 2O₂ structures as active sites for the MTM process.

Conversion of Methane to Methanol on TM-Doped Monolayers Supported on Ni(111). Reaction energy profiles of methane oxidation on GR-Rh/Ni(111) with 2O₂ as the active site is shown in Figure 2. For the calculation of the free energy profiles, the partial pressures of CH₄, O₂, and CH₃OH were set to 50, 1, and 1 bar, respectively. The temperature was set to 473 K.¹ Starting from O₂-a (IS, Figure

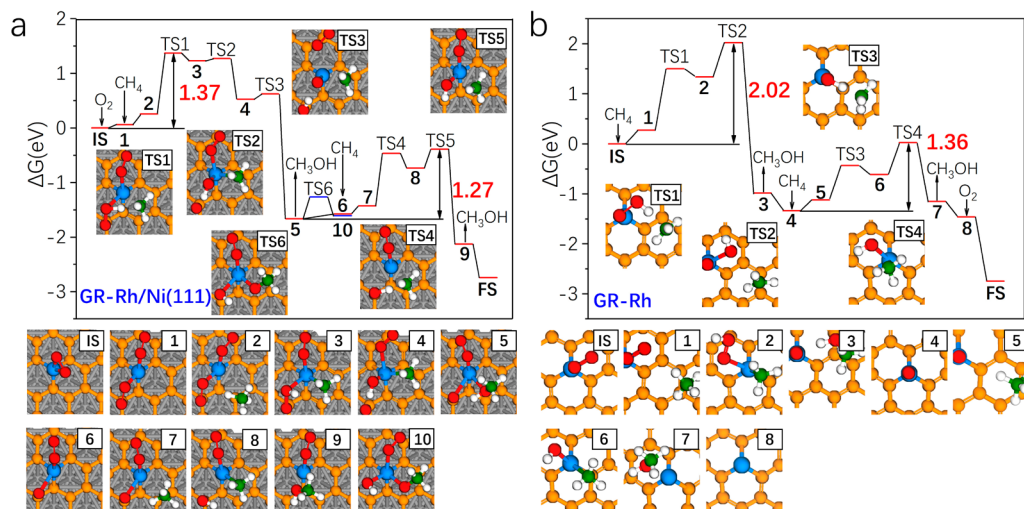


Figure 2. Pressure corrected ($P_{O_2} = 1$ bar, $P_{CH_4} = 50$ bar, $P_{CH_3OH} = 1$ bar) free energy profiles at 473 K associated with the configurations of each intermediate and transition state for the methane partial oxidation over (a) GR-Rh/Ni(111), $2O_2$ configuration is the active species; (b) GR-Rh. IS and FS denote initial and final state, respectively. The energetics of each state is also provided in [Tables S2 and S3](#). Hydrogen is shown in white; the carbon atom pertaining to CH_4 is shown in green.

2a), one additional O_2 is adsorbed to form the active site (1), which is endergonic by 0.06 eV. Next, methane physisorbs on GR-Rh/Ni(111) (2), which subsequently can react with the two oxygen atoms of the adsorbed O_2 with a bond length of 1.461 Å (while the other adsorbed O_2 with an O–O bond length of 1.288 Å is a bystander during the reaction). For the reaction with the first oxygen atom, breaking of the C–H bond occurs concurrently with formation of an O–H bond on GR-Rh/Ni(111), the formation of a Rh–C bond, and a further elongation of the O–O bond to 1.505 Å (2 → 3). The first reaction step occurs with a reasonably low free energy barrier of 1.12 eV (Figure 2a). We also considered the dissociation of O_2 before reacting with methane. However, we did not obtain a stable configuration with a broken O–O bond. The breaking of the O–O bond (3 → 4) only requires overcoming a small barrier of 0.04 eV. The formation of the first CH_3OH (4 → 5) also occurs readily with a free energy barrier of 0.09 eV, which can be explained by the high exergonicity of this elementary step (−2.19 eV). Subsequent desorption of CH_3OH is slightly endergonic by 0.08 eV (5 → 6), significantly facilitating the often-challenging methanol removal step typical of Cu-exchanged zeolites.³ The second oxygen then reacts with another CH_4 by overcoming a free energy barrier of 0.96 eV (7 → 8). The second CH_3OH is formed upon association of the CH_3 and OH species (8 → 9). Finally, upon the desorption of the second CH_3OH (9 → FS) the catalytic cycle is closed. Apart from the methanol formation mechanism, O–H bond breaking of the adsorbed methanol can also occur (5 → 10), forming an adsorbed methoxy and hydroxyl that in some catalyst systems (see below), but not on GR-Rh/Ni(111) as shown in Figure 2, can poison the active site. The entire MTM process has an effective barrier of 1.37 eV, corresponding to the first CH_4 activation process. As CH_4 is only physisorbed at the active center with preadsorbed O_2/O , the MTM mechanism can be described as an Eley–Rideal mechanism.

The energy profile of the MTM process occurring at O_2 -b, which features a chemisorbed O_2 at the interfacial site with an O–O bond length of 1.478 Å, is presented in Figure S1. While the methane C–H activation and the formation of methanol can readily occur, the effective barrier of the reaction amounts

to 1.62 eV since the free energy of the O_2 -b site is 0.50 eV higher than that of O_2 -a. Starting from O_2 -a, where O_2 is adsorbed over Rh, both the first methane C–H cleavage and the methanol formation step are difficult with an effective barrier of 1.74 eV (Figure S2). The high barrier can be explained by two aspects: (1) the O_2 of O_2 -a is activated to a lesser extent than that at an interfacial site and there is an energy penalty to further reduce O_2 ; (2) O_2 binds with Rh strongly and CH_3 has to compete with O_2 for the adsorption site. Since the high effective barrier of the first methanol formation process for O_2 -a is even higher than that of O_2 -b, we did not examine the second methanol formation process for O_2 -a.

Interestingly, the CH_4 activation process is dramatically different for free-standing GR-Rh (Figure 2b). A O_2 molecule only binds with Rh through a η^2 mode and the O–O bond length is elongated to 1.360 Å upon adsorption (Figure 1b). The effective barrier of the entire process was calculated to be 2.02 eV, which occurs at the formation of the first methanol elementary step (2 → 3). The very different free energy profile of the Ni(111)-supported and free-standing GR-Rh highlights the critical role of the metal support for the MTM reaction.

As Cu-exchanged zeolites are among the most extensively explored catalysts for MTM conversion, we also examined Cu for TM-doped GR supported on Ni(111) as a candidate of a MTM catalyst. Preferred O_2 adsorption configurations under reaction conditions were determined by constrained thermodynamics calculations (Figure S3). With the most stable configuration of two O_2 adsorbed on GR-Cu/Ni(111), we found that the effective barrier of the first C–H cleavage is 1.62 eV (Figure S4), significantly higher than the effective barrier of 1.37 eV for the entire process on GR-Rh/Ni(111). An energy barrier difference of 0.25 eV suggests a ∼460 times lower reaction rate at 473 K. Therefore, GR-Cu/Ni(111) is not a good candidate as a MTM catalyst.

We also examined the energy profile of the MTM on Rh-doped hBN. Three O_2 can adsorb neighboring the Rh dopant at operating conditions (Figure S5). While methane activation and methanol formation can occur on hBN-Rh/Ni(111) with an effective barrier of only 1.31 eV, methoxy species (9) can be formed easier than methanol and is highly stable, rendering the

Table 1. Bond Lengths and Bader Charges of TS(CH₄) and TS(CH₃OH) on the First and Second Surface Oxygen on GR-Rh/Ni(111)^a

	first oxygen				second oxygen	
	TS(CH ₄)	TS(CH ₃ OH)	TS(CH ₄)	TS(CH ₃ OH)	TS(CH ₄)	TS(CH ₃ OH)
bond length (Å)	O–H	1.185	O1–H1	1.204	O–H	1.208
	C–H	1.498	C–H	1.476	C–H	1.478
	Rh–C	2.340	Rh–C	2.418	Rh–C	2.346
Bader charge (le ^{−1})			O2–H2	2.001		O2–H2
	Rh	0.76	Rh	0.75	Rh	0.70
	C	−0.50	C	0.17	C	−0.52
			O2	−0.29		O2
			H2	0.74		H2

^aAtoms are labelled identically to those in Figure 3.

effective barrier of the second methanol formation step to be 2.05 eV and poisoning the catalyst (Figure S6).

Owing to the electronic perturbation of the Rh-doped GR monolayer by the presence of the Ni(111) support, impressive catalytic activities for methane partial oxidation are predicted that are nonexistent for the free-standing counterparts. The interaction between the Rh-doped GR and Ni(111) that enables the catalytic properties of Rh-doped GR is termed as electronic atomic monolayer–metal support interaction (EAMSI) which is distinct from the classical strong metal–support interaction¹⁴ or electronic metal–support interaction.¹⁵ The previously reported electronic interaction between graphene and encapsulated TMs^{22,23,38} that can lead to desired catalytic activities falls likely also into our definition of EAMSI. We will demonstrate the general nature of EAMSI in the next section by illustrating more examples of tunability of probe molecule adsorption energies on TM-doped monolayers when these are chemisorbed on a Ni(111) support.

Next, we developed a microkinetic model for the MTM reaction to better understand the reaction kinetics of the GR-Rh/Ni(111) catalyst (details in the Supporting Information). At 473 K, the turnover frequency for Rh-hBN/Ni(111) was calculated to be 0.017/s. The apparent activation energy for the catalyst was found to be 0.59 eV (Figure S7). A reaction order of 1 and 0.54 was obtained for CH₄ (1–50 bar) and O₂ (1–5 bar). The rate controlling step (first CH₄ C–H cleavage) was identified using Campbell's degree of rate control (DRC) and thermodynamic rate control (TRC) analysis³⁹ and all degrees of rate control are listed in Table S4.

An important concern regarding methane partial oxidation is the selectivity to methanol since the C–H bond energy of methanol is 0.49 eV lower than that of methane and hence, overoxidation of methanol is possible.¹ Conventional scaling relationships, correlating the activation energies of C–H dissociation and H adsorption energies, suggest that the energy barrier of the methane C–H bond is ~0.55 eV higher than that of methanol.² To circumvent the undesired overoxidation of methanol, it has been proposed to mix an adsorbent with strong adsorption energy for methanol with the catalyst to effectively reduce the partial pressure of methanol.⁴⁰ In the present study, however, we found that the transition state (TS) DFT energies for the first and second CH₄ C–H cleavage is only 0.13 and 0.08 eV higher than that of CH₃OH occurring at the same adsorption site, respectively, breaking the scaling relationships of the TS energies for methane and methanol C–H bond activation.² Under reaction conditions of a CH₄ partial pressure of 50 bar and a CH₃OH partial pressure of 1 bar, the free energies of the C–H bond cleavage TSs in

CH₄ for the first and second surface oxygen are 0.19 and 0.22 eV lower than those for the C–H bond cleavage TSs in CH₃OH. CH₄ C–H breaking is preferred by ~0.04 eV over that of CH₃OH even when the two molecules have the same partial pressure (Figure S8). As such, overoxidation of methanol can be avoided at significant methane conversion. To understand the unusual selectivity toward methane C–H activation, we plotted the spin density of each TS structure and found that no spin density is localized at the carbon atom (Figure S9). Therefore, these TS structures are not radicals, different to what is assumed in the well-accepted C–H activation scaling relationship.² We also analyzed the bond lengths and Bader charges of the TS structures (Table 1). In contrast to the conventional radical-like TS² where the CH₃-group (or CH₂OH-group for the TS of CH₃OH) is only tethered to one surface oxygen atom, the CH₃ (CH₂OH) of the TSs of the present study are stabilized by both the surface oxygen and the neighboring Rh with the Rh–C distance being ~2.4 Å. As revealed by Bader analysis, both C–H dissociation TS structures for CH₃OH have a slightly positively charged carbon atom due to the neighboring OH group. In contrast, both C–H dissociation TS structures for CH₄ have a negatively charged carbon atom of ca. −0.5 le^{−1} since carbon is more electronegative than hydrogen. The repulsive electrostatic C–Rh interactions for the CH₃OH TS and attractive C–Rh interactions for the CH₄ TS lead to a significantly narrowed energy difference between the CH₃OH and CH₄ TSs. This observation is also consistent with the shorter C–Rh distance for the two CH₄ TS structures. Here, we note that the O2–H2 (see Figure 3) bond distances for both CH₃OH TS structures are ~2 Å such that also the hydrogen bond stabilization in the CH₃OH TS structures is very weak. Overall, the synergy of the oxygen and the neighboring cationic Rh leads to the stabilization (destabilization) of the TS for CH₄ (CH₃OH).

Tuning the Adsorption Energies of Probe Molecules by EAMSI. We further explored the universality of changing the adsorption strength of various molecules on TM-doped 2D materials by chemisorption on Ni(111). Cu, Fe, Ir, Mn, and Rh are common active elements in heterogeneous catalysis and were therefore tested for doping graphene, hBN, and N-doped graphene featuring a MN₄ motif (Figure 4d). The study of TM atoms immobilized in N-doped graphene featuring a MN₄ motif is a recently emerging topic in single-atom electrocatalysis.^{27,41} Figure 4a lists the adsorption energies of these TM-doped monolayers on Ni(111). Next, the adsorption strength of CO, C₂H₄, and OH were examined for TM-doped GR (Figure 4b). In general, the presence of the Ni(111) support has a noticeable effect on the adsorption energy. For

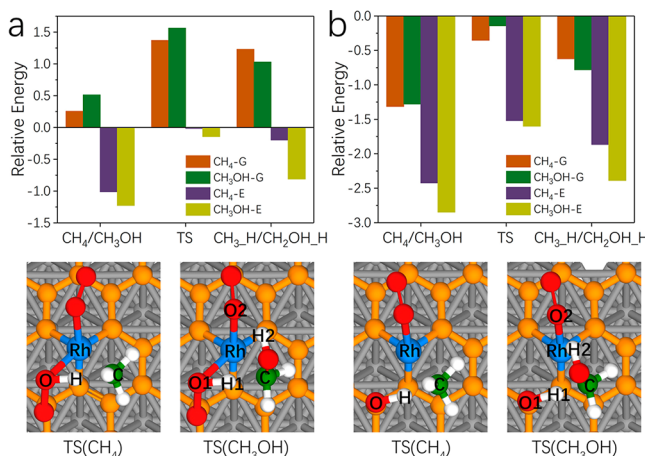


Figure 3. DFT energy and free energy ($T = 473 \text{ K}$, $P_{\text{O}_2} = 1 \text{ bar}$, $P_{\text{CH}_4} = 50 \text{ bar}$, $P_{\text{CH}_3\text{OH}} = 1 \text{ bar}$) profile for CH_4 and CH_3OH C–H breaking by the first (a) and second (b) surface oxygen on GR-Rh/Ni(111). G denotes free energy, and E denotes DFT energy. The reference states are set to be the IS in Figure 2 and the corresponding gas molecules.

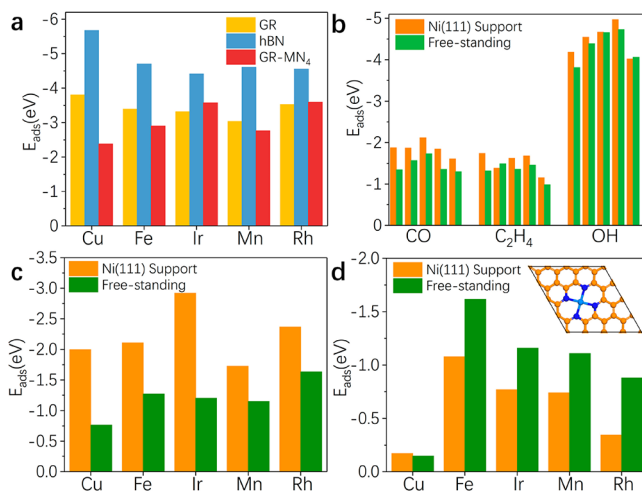


Figure 4. (a) Adsorption energies of Cu-, Fe-, Ir-, Mn-, and Rh-doped GR, hBN, and GR-MN₄ on (4 × 4) Ni(111). (b) Adsorption energies of CO, C₂H₄, and OH on Ni(111) supported Cu-, Fe-, Ir-, Mn-, and Rh-doped GR as well as the free-standing ones. (c) Adsorption energies of CO on TM-doped hBN. (d) Adsorption energies of CO on MN₄-embedded graphene. The insets in display the configuration of RhN₄-graphene.

example, the E_{ads} of CO on GR-Cu/Ni(111) and GR-Cu is -1.87 and -1.34 eV, respectively. Also, the E_{ads} of C₂H₄ on GR-Ir/Ni(111) is -1.62 eV compared with -1.36 eV on GR-Ir. The fact that Ni(111) can regulate the adsorption energies of OH also has important implications for the design of ORR catalysts, where the OH adsorption energy is a common descriptor of ORR activity.⁴² This is consistent with a very recent study by Mao et al.³⁰ The adsorption of CO is used to probe the properties of Ni(111)-supported and free-standing TM-doped hBN (Figure 4c) and graphene-MN₄ (Figure 4d). All of these results suggest that the presence of a metal support that forms covalent bonds with the TM-doped atomic monolayer can regulate the adsorption energy of small molecules on the TM-dopant. Therefore, it is possible to tune the catalytic properties of SACs by harnessing EAMSI that could possibly modify the adsorption strength of

intermediate and transition state structures. Up to now, we only considered the cases of monometallic Ni(111)-supported monolayers. The adsorption energy of a molecule can also be tuned by doping Ni(111) with a heteroatom. When a Ni atom underneath a dopant-bonded N in hBN is replaced with Cu (Figure S10), the E_{ads} for CO on hBN-Cu/Ni(111) is -1.82 eV, as compared with the pristine Ni(111) case of -2.00 eV. The diversity of atomic monolayers, TM dopants, and metal supports opens enormous opportunities for design of SACs.

CONCLUSIONS

We propose a novel electronic atomic monolayer–metal support interaction (EAMSI) that enables the activation of dioxygen upon adsorption, which in turn leads to the activation of methane through an Eley–Rideal reaction mechanism. GR-Rh/Ni(111) exhibits a high activity for methane partial oxidation. The high activity can be traced back to the presence of interfacial oxygen on GR-Rh/Ni(111), which is activated by Rh and graphene C atoms. The conventional C–H activation scaling relationship that predicts a TS energy difference of ~ 0.55 eV between CH_4 and CH_3OH is broken, leading to a significantly narrowed energy difference. The breaking of the scaling relationship is due to the synergy of adsorbed activated oxygen atoms on the surface and a neighboring cationic Rh atom that electrostatically attracts (repels) the methane (methanol) carbon atom in the C–H transition state, a mechanism that can likely more generally be used for the design of MTM catalysts with minimal overoxidation of methanol.

Overall, the proposed GR-Rh/Ni(111) catalyst can potentially overcome various issues of typical Cu-exchanged zeolite MTM catalysts such as the necessity of catalyst preoxidation, low activity and methane conversion as well as strong adsorption of methanol. Finally, the properties of Ni(111)-supported monolayers and free-standing 2D materials were probed with the adsorption of several small molecules. The feasibility of tuning the adsorption energy of various probe molecules with EAMSI represents a new paradigm for tuning the properties of atomic monolayer-based single-site catalysts that have great structural and compositional diversity.

METHODS

First-principles calculations were performed using periodic density functional theory (DFT), as implemented in the Vienna Ab initio Simulation Package (VASP 5.4.4).^{43,44} The spin-polarized generalized gradient approximation (GGA) with the PBE functional⁴⁵ was used to treat exchange–correlation effects. A plane wave basis set with a cutoff energy of 400 eV was selected to describe the valence electrons. The electron–ion interactions were described by the projector augmented wave (PAW)^{46,47} method. The Brillouin zone integration was performed with a $3 \times 3 \times 1$ Monkhorst–Pack⁴⁸ (MP) k-mesh and Gaussian smearing ($\sigma = 0.1$ eV). We used Grimme's DFT-D⁴⁹ scheme to include the van der Waals interactions semiempirically. The SCF and force convergence criteria for structural optimization were set to 1×10^{-5} eV and 0.01 eV/Å, respectively. The climbing image nudged elastic band (CI-NEB)⁵⁰ and dimer methods^{51,52} were used to optimize the transition state structures. The force convergence criterion for transition state optimization was set to be 0.03 eV/Å. A five-layer 4 × 4 Ni(111) slab was used to describe the Ni slab and

neighboring slabs were separated by a 13 Å vacuum. Harmonic transition state theory was used to calculate all elementary rate constants of surface processes. Collision theory with a sticking coefficient of 1 was used to estimate the rate constants for adsorption processes. Details of rate constant calculations and the microkinetic model are provided in the *Supporting Information*. In all models, we applied the standard correction to the O–O bonding energy⁵³ as detailed in the *Supporting Information*. The adsorption energy of a gas phase molecule is defined as $E_{\text{ads}} = E(\text{surface} + \text{adsorbent}) - E(\text{surface}) - E(\text{adsorbent})$. The adsorption energy of a metal atom is defined as $E_{\text{ads}} = E(\text{surface} + \text{atom}) - E(\text{surface}) - E(\text{atom from bulk metal})$.

■ ASSOCIATED CONTENT

Supporting Information

The Supporting Information is available free of charge on the ACS Publications website at DOI: [10.1021/acscatal.9b01619](https://doi.org/10.1021/acscatal.9b01619).

Alternative energy profiles of methane partial oxidation over GR-Rh/Ni(111); methane C–H activation over GR-Cu/Ni(111); methane partial oxidation over hBN-Rh/Ni(111); Arrhenius plot; transition state free energies of C–H breaking for CH₄ and CH₃OH at various pressures; spin density of transition states for CH₄ and CH₃OH C–H bond breaking; CO adsorption on Cu-doped hBN supported on Cu-doped Ni(111); details of the microkinetic model; atomic coordinates of each transition and intermediates for reaction over GR-Rh/Ni(111) (PDF)

■ AUTHOR INFORMATION

Corresponding Author

*E-mail: heyden@cec.sc.edu.

ORCID

Andreas Heyden: [0000-0002-4939-7489](https://orcid.org/0000-0002-4939-7489)

Author Contributions

Y.X. performed the DFT calculations. Both Y.X. and A.H. participated in the discussion of the results and writing of the manuscript.

Notes

The authors declare no competing financial interest.

■ ACKNOWLEDGMENTS

We gratefully acknowledge financial support from the National Science Foundation (OIA-1632824). The research was performed using computing resources from EMSL (Ringgold ID 130367, Grant Proposal 49246), a DOE Office of Science User Facility sponsored by the Office of Biological and Environmental Research and the National Energy Research Scientific Computing Center, a DOE Office of Science User Facility supported by the Office of Science of the U.S. Department of Energy under Contract No. DE-AC02-05CH11231.

■ REFERENCES

- (1) Ravi, M.; Ranocchiari, M.; van Bokhoven, J. A. The Direct Catalytic Oxidation of Methane to Methanol—A Critical Assessment. *Angew. Chem., Int. Ed.* **2017**, *56*, 16464–16483.
- (2) Latimer, A. A.; Kulkarni, A. R.; Aljama, H.; Montoya, J. H.; Yoo, J. S.; Tsai, C.; Abild-Pedersen, F.; Studt, F.; Norskov, J. K. Understanding trends in C–H bond activation in heterogeneous catalysis. *Nat. Mater.* **2017**, *16*, 225–229.
- (3) Tomkins, P.; Ranocchiari, M.; van Bokhoven, J. A. Direct Conversion of Methane to Methanol under Mild Conditions over Cu-Zeolites and beyond. *Acc. Chem. Res.* **2017**, *50*, 418–425.
- (4) Grundner, S.; Markovits, M. A. C.; Li, G.; Tromp, M.; Pidko, E. A.; Hensen, E. J. M.; Jentys, A.; Sanchez-Sanchez, M.; Lercher, J. A. Single-site trinuclear copper oxygen clusters in mordenite for selective conversion of methane to methanol. *Nat. Commun.* **2015**, *6*, 7546.
- (5) Li, G.; Vassilev, P.; Sanchez-Sanchez, M.; Lercher, J. A.; Hensen, E. J. M.; Pidko, E. A. Stability and reactivity of copper oxo-clusters in ZSM-5 zeolite for selective methane oxidation to methanol. *J. Catal.* **2016**, *338*, 305–312.
- (6) Narsimhan, K.; Iyoki, K.; Dinh, K.; Román-Leshkov, Y. Catalytic Oxidation of Methane into Methanol over Copper-Exchanged Zeolites with Oxygen at Low Temperature. *ACS Cent. Sci.* **2016**, *2*, 424–429.
- (7) Zhao, Z.-J.; Kulkarni, A.; Vilella, L.; Nørskov, J. K.; Studt, F. Theoretical Insights into the Selective Oxidation of Methane to Methanol in Copper-Exchanged Mordenite. *ACS Catal.* **2016**, *6*, 3760–3766.
- (8) Pappas, D. K.; Borfecchia, E.; Dyballa, M.; Pankin, I. A.; Lomachenko, K. A.; Martini, A.; Signorile, M.; Teketel, S.; Arstad, B.; Berlier, G.; Lamberti, C.; Bordiga, S.; Olsbye, U.; Lillerud, K. P.; Svelle, S.; Beato, P. Methane to Methanol: Structure-Activity Relationships for Cu-CHA. *J. Am. Chem. Soc.* **2017**, *139*, 14961–14975.
- (9) Shan, J.; Li, M.; Allard, L. F.; Lee, S.; Flytzani-Stephanopoulos, M. Mild oxidation of methane to methanol or acetic acid on supported isolated rhodium catalysts. *Nature* **2017**, *551*, 605.
- (10) Bruix, A.; Rodriguez, J. A.; Ramirez, P. J.; Senanayake, S. D.; Evans, J.; Park, J. B.; Stacchiola, D.; Liu, P.; Hrbek, J.; Illas, F. A new type of strong metal-support interaction and the production of H₂ through the transformation of water on Pt/CeO₂(111) and Pt/CeO(x)/TiO₂(110) catalysts. *J. Am. Chem. Soc.* **2012**, *134*, 8968–74.
- (11) Saleheen, M.; Heyden, A. Liquid-Phase Modeling in Heterogeneous Catalysis. *ACS Catal.* **2018**, *8*, 2188–2194.
- (12) Welborn, V. V.; Ruiz Pestana, L.; Head-Gordon, T. Computational optimization of electric fields for better catalysis design. *Nat. Catal.* **2018**, *1*, 649.
- (13) Voiry, D.; Yamaguchi, H.; Li, J.; Silva, R.; Alves, D. C. B.; Fujita, T.; Chen, M.; Asefa, T.; Shenoy, V. B.; Eda, G.; Chhowalla, M. Enhanced catalytic activity in strained chemically exfoliated WS₂ nanosheets for hydrogen evolution. *Nat. Mater.* **2013**, *12*, 850–855.
- (14) Tauster, S. J. Strong metal-support interactions. *Acc. Chem. Res.* **1987**, *20*, 389–394.
- (15) Campbell, C. T. Catalyst-support interactions: Electronic perturbations. *Nat. Chem.* **2012**, *4*, 597–598.
- (16) Rodriguez, J. A.; Liu, P.; Graciani, J.; Senanayake, S. D.; Grinter, D. C.; Stacchiola, D.; Hrbek, J.; Fernandez-Sanz, J. Inverse Oxide/Metal Catalysts in Fundamental Studies and Practical Applications: A Perspective of Recent Developments. *J. Phys. Chem. Lett.* **2016**, *7*, 2627–39.
- (17) Pacchioni, G.; Giordano, L.; Baistrocchi, M. Charging of metal atoms on ultrathin MgO/Mo(100) films. *Phys. Rev. Lett.* **2005**, *94*, 226104.
- (18) Geim, A. K.; Novoselov, K. S. The rise of graphene. *Nat. Mater.* **2007**, *6*, 183–191.
- (19) Castro Neto, A. H.; Guinea, F.; Peres, N. M. R.; Novoselov, K. S.; Geim, A. K. The electronic properties of graphene. *Rev. Mod. Phys.* **2009**, *81*, 109–162.
- (20) Deng, D.; Novoselov, K. S.; Fu, Q.; Zheng, N.; Tian, Z.; Bao, X. Catalysis with two-dimensional materials and their heterostructures. *Nat. Nanotechnol.* **2016**, *11*, 218–30.
- (21) Machado, B. F.; Serp, P. Graphene-based materials for catalysis. *Catal. Sci. Technol.* **2012**, *2*, 54–75.
- (22) Guo, N.; Xi, Y.; Liu, S.; Zhang, C. Greatly Enhancing Catalytic Activity of Graphene by Doping the Underlying Metal Substrate. *Sci. Rep.* **2015**, *5*, 12058.
- (23) Cui, X.; Ren, P.; Deng, D.; Deng, J.; Bao, X. Single layer graphene encapsulating non-precious metals as high-performance

electrocatalysts for water oxidation. *Energy Environ. Sci.* **2016**, *9*, 123–129.

(24) Ambrosetti, A.; Silvestrelli, P. L. Enhanced chemical reactivity of graphene on a Ni(111) substrate. *J. Chem. Phys.* **2016**, *144*, 111101.

(25) Yan, H.; Zhao, X.; Guo, N.; Lyu, Z.; Du, Y.; Xi, S.; Guo, R.; Chen, C.; Chen, Z.; Liu, W.; Yao, C.; Li, J.; Pennycook, S. J.; Chen, W.; Su, C.; Zhang, C.; Lu, J. Atomic engineering of high-density isolated Co atoms on graphene with proximal-atom controlled reaction selectivity. *Nat. Commun.* **2018**, *9*, 3197.

(26) Kirk, C.; Chen, L. D.; Siahrostami, S.; Karamad, M.; Bajdich, M.; Voss, J.; Nørskov, J. K.; Chan, K. Theoretical Investigations of the Electrochemical Reduction of CO on Single Metal Atoms Embedded in Graphene. *ACS Cent. Sci.* **2017**, *3*, 1286–1293.

(27) Guan, J. Q.; Duan, Z. Y.; Zhang, F. X.; Kelly, S. D.; Si, R.; Dupuis, M.; Huang, Q. G.; Chen, J. Q.; Tang, C. H.; Li, C. Water oxidation on a mononuclear manganese heterogeneous catalyst. *Nat. Catal.* **2018**, *1*, 870–877.

(28) Qiao, B.; Wang, A.; Yang, X.; Allard, L. F.; Jiang, Z.; Cui, Y.; Liu, J.; Li, J.; Zhang, T. Single-atom catalysis of CO oxidation using Pt1/FeOx. *Nat. Chem.* **2011**, *3*, 634–641.

(29) Wang, A. Q.; Li, J.; Zhang, T. Heterogeneous single-atom catalysis. *Nat. Rev. Chem.* **2018**, *2*, 65–81.

(30) Mao, X.; Kour, G.; Yan, C.; Zhu, Z.; Du, A. Single Transition Metal Atom-Doped Graphene Supported on a Nickel Substrate: Enhanced Oxygen Reduction Reactions Modulated by Electron Coupling. *J. Phys. Chem. C* **2019**, *123*, 3703–3710.

(31) Dahal, A.; Batzill, M. Graphene-nickel interfaces: a review. *Nanoscale* **2014**, *6*, 2548–2562.

(32) Muntwiler, M.; Auwärter, W.; Baumberger, F.; Hoesch, M.; Greber, T.; Osterwalder, J. Determining adsorbate structures from substrate emission X-ray photoelectron diffraction. *Surf. Sci.* **2001**, *472*, 125–132.

(33) Jin, C.; Lin, F.; Suenaga, K.; Iijima, S. Fabrication of a Freestanding Boron Nitride Single Layer and Its Defect Assignments. *Phys. Rev. Lett.* **2009**, *102*, 195505.

(34) Gan, Y.; Sun, L.; Banhart, F. One- and Two-Dimensional Diffusion of Metal Atoms in Graphene. *Small* **2008**, *4*, 587–591.

(35) Zhang, L.; Jia, Y.; Gao, G.; Yan, X.; Chen, N.; Chen, J.; Soo, M. T.; Wood, B.; Yang, D.; Du, A.; Yao, X. Graphene Defects Trap Atomic Ni Species for Hydrogen and Oxygen Evolution Reactions. *Chem.* **2018**, *4*, 285–297.

(36) Henkelman, G.; Arnaldsson, A.; Jonsson, H. A fast and robust algorithm for Bader decomposition of charge density. *Comput. Mater. Sci.* **2006**, *36*, 354–360.

(37) Romero-Muñiz, C.; Martín-Recio, A.; Pou, P.; Gómez-Rodríguez, J. M.; Pérez, R. Substrate-induced enhancement of the chemical reactivity in metal-supported graphene. *Phys. Chem. Chem. Phys.* **2018**, *20*, 19492–19499.

(38) Deng, J.; Ren, P.; Deng, D.; Bao, X. Enhanced electron penetration through an ultrathin graphene layer for highly efficient catalysis of the hydrogen evolution reaction. *Angew. Chem., Int. Ed.* **2015**, *54*, 2100–4.

(39) Campbell, C. T. The Degree of Rate Control: A Powerful Tool for Catalysis Research. *ACS Catal.* **2017**, *7*, 2770–2779.

(40) Latimer, A. A.; Kakekhani, A.; Kulkarni, A. R.; Nørskov, J. K. Direct Methane to Methanol: The Selectivity-Conversion Limit and Design Strategies. *ACS Catal.* **2018**, *8*, 6894–6907.

(41) Fei, H.; Dong, J.; Feng, Y.; Allen, C. S.; Wan, C.; Voloskiy, B.; Li, M.; Zhao, Z.; Wang, Y.; Sun, H.; An, P.; Chen, W.; Guo, Z.; Lee, C.; Chen, D.; Shakir, I.; Liu, M.; Hu, T.; Li, Y.; Kirkland, A. I.; Duan, X.; Huang, Y. General synthesis and definitive structural identification of MN4C4 single-atom catalysts with tunable electrocatalytic activities. *Nat. Catal.* **2018**, *1*, 63–72.

(42) Kulkarni, A.; Siahrostami, S.; Patel, A.; Nørskov, J. K. Understanding Catalytic Activity Trends in the Oxygen Reduction Reaction. *Chem. Rev.* **2018**, *118*, 2302–2312.

(43) Kresse, G.; Furthmüller, J. Efficient iterative schemes for ab initio total-energy calculations using a plane-wave basis set. *Phys. Rev. B: Condens. Matter Mater. Phys.* **1996**, *54*, 11169.

(44) Kresse, G.; Furthmüller, J. Efficiency of ab-initio total energy calculations for metals and semiconductors using a plane-wave basis set. *Comput. Mater. Sci.* **1996**, *6*, 15–50.

(45) Perdew, J. P.; Burke, K.; Ernzerhof, M. Generalized gradient approximation made simple. *Phys. Rev. Lett.* **1996**, *77*, 3865.

(46) Blöchl, P. E. Projector augmented-wave method. *Phys. Rev. B: Condens. Matter Mater. Phys.* **1994**, *50*, 17953–17979.

(47) Kresse, G.; Joubert, D. From ultrasoft pseudopotentials to the projector augmented-wave method. *Phys. Rev. B: Condens. Matter Mater. Phys.* **1999**, *59*, 1758–1775.

(48) Monkhorst, H. J.; Pack, J. D. Special Points for Brillouin-Zone Integrations. *Phys. Rev. B* **1976**, *13*, 5188.

(49) Grimme, S.; Antony, J.; Ehrlich, S.; Krieg, H. A consistent and accurate ab initio parametrization of density functional dispersion correction (DFT-D) for the 94 elements H–Pu. *J. Chem. Phys.* **2010**, *132*, 154104.

(50) Henkelman, G.; Uberuaga, B. P.; Jonsson, H. A climbing image nudged elastic band method for finding saddle points and minimum energy paths. *J. Chem. Phys.* **2000**, *113*, 9901–9904.

(51) Henkelman, G.; Jónsson, H. A dimer method for finding saddle points on high dimensional potential surfaces using only first derivatives. *J. Chem. Phys.* **1999**, *111*, 7010–7022.

(52) Heyden, A.; Bell, A. T.; Keil, F. J. Efficient methods for finding transition states in chemical reactions: comparison of improved dimer method and partitioned rational function optimization method. *J. Chem. Phys.* **2005**, *123*, 224101.

(53) Wang, L.; Maxisch, T.; Ceder, G. Oxidation energies of transition metal oxides within the GGA+U framework. *Phys. Rev. B: Condens. Matter Mater. Phys.* **2006**, *73*, 195107.